Colloidal Stability of Imogolite Nanotube Dispersions: A Phase Diagram Study

Erwan Paineau, Geoffrey Monet, Véronique Peyre, Claire Goldmann, Stéphan Rouzière, Pascale Launois

Colloidal Stability of Imogolite Nanotubes Dispersions: A Phase Diagram Study

Erwan Paineau,[a,*] *Geoffrey Monet,*[a] *Véronique Peyre,*[b] *Claire Goldmann,*[a] *Stéphan Rouzière,*[a] *Pascale Launois*[a]

[a] Laboratoire de Physique des Solides, UMR CNRS 8502, Univ. Paris-Sud, Université Paris-Saclay, Bâtiment 510, 91405 Orsay, France.

[b] PHENIX, UMR CNRS 8234, Sorbonne Universités, UPMC Univ. Paris 06, 75005 Paris, France.

*E-mail: erwan-nicolas.paineau@u-psud.fr

ABSTRACT. In this article, we revisit the colloidal stability of clay imogolite nanotubes by studying the effect of electrostatic interactions on geo-inspired synthetic nanotubes in aqueous dispersions. The nanotubes in question are double-walled aluminogermanate imogolite nanotubes (Ge-DWINTs) with a well-defined diameter (4.3 nm) and with an aspect ratio around 4. Surface charge properties are assessed by electrophoretic measurements, revealing that the outer surfaces of Ge-DWINT are positively charged up to high pH values. Series of Ge-DWINT dispersions have been prepared by osmotic stress to control both ionic strength of the dispersion and the volume fraction in nanotubes. Optical observations coupled to Small and Wide-Angle X-ray Scattering (SAXS/WAXS) experiments allow us to unravel different nanotube organizations. At low ionic strength (IS < 10^{-2} mol.L^{-1}), Ge-DWINTs are fully dispersed in water while they form an arrested gel phase above a given concentration threshold, which shifts towards higher volume fraction with increasing ionic strength. The swelling law, derived from the evolution of the mean intertube distance as a function of the nanotube concentration, evidences a transition from isotropic swelling at low volume fractions to one-dimensional swelling at higher volume fractions. These results show that the colloidal stability of Ge-DWINT is driven by repulsive interactions for ionic strengths lower than 10^{-2} mol.L^{-1}. By contrast, higher salt concentrations lead to attractive interactions that destabilize the colloid suspension, inducing nanotube coagulation into larger structures that settle over time or form opaque gels. Detailed simulations of the WAXS diagram reveal that aggregates are mainly formed by an isotropic distribution of small bundles (less than 4 nanotubes) in which the nanotubes organized themselves in parallel orientation. Altogether, these measurements allow us to give the first overview of the phase diagram of colloidal dispersions based on geo-inspired imogolite-like nanotubes.

INTRODUCTION

The state of dispersions of clay nanoparticles is important in many industrial applications, from the production of nanocomposites to food packaging,[1] and it is also involved in various environmental processes.[2] When one refers to the colloidal properties of clays, it usually concerns properties related to swelling clay nanosheets.[3,4] Since the pioneering work of Langmuir,[5] a wide literature has been devoted to the colloidal stability of di- or trioctahedral swelling clay minerals such as smectites and hectorites.[6–14] These charged clay nanosheets exhibit a wide variety of states (isotropic sols, liquid-crystal phases, repulsive and attractive arrested phases, flocs and aggregated sediments) depending not only on the size of the clay particles or the effect of charge location, but also on the ionic strength *IS* of the solution ($IS = \frac{1}{2}\sum_{i=0}^{n} c_i z_i^2$, where the sum performed over all types 'i' of ions of the solution, with concentration c_i and with charge z_i, is simply equal to the concentration of monovalent ions here), the valence and hydration properties of ions in the suspension.[15–20] Compared to this large body of literature, there is surprisingly few works dealing with the colloidal stability of one-dimensional clay particles such as sepiolite nanorods[21] or halloysite nanotubes.[22] It might be related to the challenges of stabilizing in aqueous media this type of anisometric objects that remain stable for only few hours. Different strategies have been therefore employed to extend colloidal stability, either by adsorption of anionic compounds or dispersion in hexametaphosphate.[22–24]

Imogolite-like nanotubes (INTs) offer an interesting alternative since these aluminosilicate and aluminogermanate nanotubes can form stable aqueous dispersions without the assistance of a stabilizing agent.[25] Belonging to clay minerals, these inorganic nanotubes consist of a curved octahedral [$Al(OH)_3$] layer on which isolated [$(Si,Ge)O_3(OH)$] tetrahedron units are connected upright to the octahedral vacancy via covalent bonding between three mutual oxygen atoms

(Figure 1a). A nanotube wall is constructed from $(OH)_3Al_2O_3(Si,Ge)(OH)$ elementary units, where hydroxyl groups and atoms are labelled here from outside to inside the wall.[26,27]

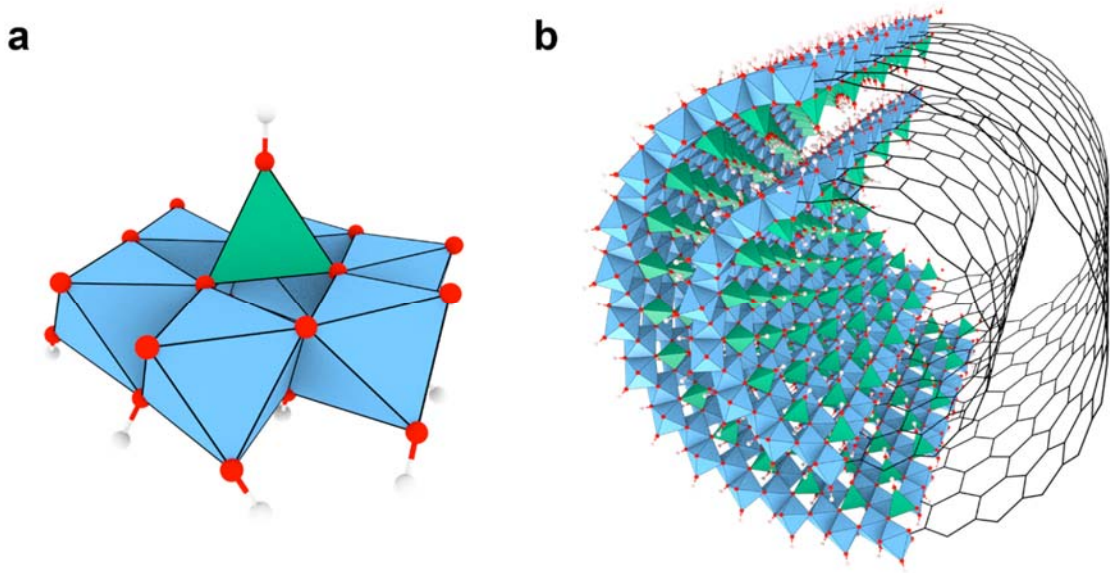

Figure 1. (a) Local arrangement of AlO_6 octahedra (in blue) and $Ge(Si)O_4$ tetrahedra (in green) in imogolite-like nanotubes; O atoms are shown in red and H ones in white. (b) Schematic view of the atomic structure of a double-walled germanium-based imogolite nanotube (Ge-DWINT). Al, blue; Ge, green; O, red; H, white.

Naturally occurring worldwide either in weathered volcanic soils or in Spodosols,[28] INTs can also be synthesized easily by using low-temperature sol-gel methods,[29] while controlling both their inner diameter (1.5-3 nm), shape (single-walled: SW; or double-walled: DW structures, Figure 1b), or surface properties.[27,30,31] Thanks to these unique behaviors, INTs are becoming appealing for a wide range of potential applications,[32,33] ranging from nanocomposites[34] to molecular filtration[35] or for energy production[36] to cite a few. Currently, it remains a very challenging task to control the packing of nanotubes before or during the processing into films, membranes or complex hierarchical structures.[37] From an applied point of view, a deep understanding of the

colloidal stability of these systems is therefore necessary since most applications start from dispersions of INTs.

The swelling and colloidal properties of these nanotubes were quickly recognized as early as their discovery as macroscopic gel-like films in weathered pumice beds.[38]Starting from INTs suspensions, it is easy to obtain individually dispersed nanotubes in acidic and low ionic strength aqueous medium.[39] However, INTs have a strong tendency to form instantaneously transparent gels or to bundle irreversibly in bulky flocs at alkaline pH or for high ionic strength.[39–42] For instance, it has long been recognized that addition of a concentrated ammonia solution (typically 30 wt%) leads to the formation of gels,[29] a straightforward method to retrieve a concentrated suspension but with potentially aggregated nanotubes at this alkaline pH. More interestingly, dispersions of INTs also show well-ordered liquid-crystalline phases for relatively low volume fraction,[25,43,44] if the nanotubes have a large enough aspect ratio. All these features are related to the surface charge properties of INTs and the peculiar difference in bond valence leading to positively (negatively) charged outer (inner) surface.[45–47] If we refer to the classical Derjaguin-Landau-Verwey-Overbeek (DLVO) theory, the colloidal stability of charged particles is a balance between repulsive electrostatic forces due to the diffuse double layer of counterions and attractive van der Waals forces. This delicate equilibrium is clearly dependent on the ionic strength of the medium. Determining the "phase diagram" as a function of the nanotube volume fraction and the suspension ionic strength is therefore essential to understand and predict the colloidal stability of INTs dispersions in aqueous medium.

This study aims to propose the first complete phase diagram of INTs dispersions. Samples are synthetic double-walled Ge-INTs (Ge-DWINTs) as schematically represented in Figure 1b. Surface charge properties are assessed thanks to electrophoretic measurements, revealing that Ge-

DWINTs outer surfaces are positively charged up to high pH values. Different suspensions have been prepared at fixed IS by osmotic stress to scan the volume fraction/IS phase diagram. Optical observations and Wide Angle X-ray Scattering (WAXS) experiments allow us to unravel different domains in this phase diagram for nanotube organization. At low ionic strength ($IS \leq 10^{-2}$ mol.L^{-1}), Ge-DWINTs are fully dispersed in aqueous suspensions while they form a gel phase above a given volume fraction threshold. By contrast, higher salt concentrations induce aggregation phenomena with the progressive formation of small bundles in suspension. These results are completed by using Small-Angle X-ray Scattering (SAXS) experiments to assess correlations between nanotubes depending on the position in the phase diagram as well as to establish a general swelling law.

EXPERIMENTAL SECTION

Chemicals. Aluminum perchlorate nonahydrate ($Al(ClO_4)_3.9H_2O$, ACS reagent, ≥ 98%), tetraethoxygermane (TEOG, ≥99.95%), anhydrous NaOH (ACS reagent, ≥ 97%), NaCl (ACS reagent, ≥ 99%), polyethylene glycol (PEG_{20000}, M = 20000 g.mol^{-1}) and ethanol solution (96%) were purchased from Sigma Aldrich. KBr (IR grade) was purchased from Merck. All products were used as received.

Synthesis of aluminogermanate double-walled nanotubes (Ge-DWINTs). Ge-DWINTs were synthesized by sol-gel process using the method proposed by Levard et al.[48] Typically, the synthesis is performed in PTFE beakers by adding $Ge(OEt)_4$ to an aluminum perchlorate solution with an [Al]/[Ge] ratio equal to 2 under vigorous stirring. In order to obtain only DW nanotube structures, the initial aluminum concentration is set at 0.25 mol.L^{-1}.[49] The solution is slowly hydrolyzed by addition of a NaOH solution (0.25 mol.L^{-1}) until a [OH]/[Al] of 2 is reached and then, this mixture is placed into an oven at 95°C for 5 days. At the end of the ageing process, the suspension was recovered at room temperature and subsequently dialyzed (Spectra/Por, cut-off 10

kDa, Spectrum) against ultrapure water until the conductivity dropped below 5 µS.cm^{-1}. The initial suspension stock will be referenced as DW_0 hereafter.

Nanotubes characterization. The characterization of synthesized nanotubes was performed from an aliquot of the DW_0 suspension. Transmission Electron Microscopy (TEM) observations on individual nanotubes were performed on a JEOL1400 microscope operating at 80 kV to avoid any electron beam damage. The use of standard procedure by depositing a drop of the dialyzed suspension on the TEM grid always leads to the formation of thread-like structures forming entangled networks of INTs.[50] To overcome this drawback, observation of individual nanotubes was achieved by simply using a modification of the method proposed by Yang & Su,[51] and Yucelen et al.[52] Typically, a dilute suspension of DW_0 (~ 1 mg.L^{-1}) was prepared in ethanol and a drop was deposited on a carbon-coated copper grid lying on an absorbent paper and dried in air. The morphological parameters, i.e. the mean length and diameter of DW_0, were measured over 500 individual particles by using Fiji software.[53] The polydispersity index PDI was also determined as:

$$PDI_X = (\langle X^2 \rangle - \langle X \rangle^2)^{1/2} / \langle X \rangle \quad (1)$$

with $\langle X \rangle$ being either the mean length L or diameter D of the nanotubes.

Fourier Transform Infrared Spectroscopy (FTIR) spectrum of DW_0 was recorded using a Nicolet iS50 FTIR spectrometer equipped with a KBr beamsplitter and a DTGS/KBr detector. The transmission measurement was performed at 4 cm^{-1} resolution in the low IR region (1300-400 cm^{-1} range). A pressed pellet was prepared by mixing about 1.5 mg of dry DW_0 powder with 150 mg of KBr.

Measurement of the electrophoretic mobility μ was undertaken using a Zetasizer Nano ZS (Malvern) at a fixed wavelength of 632 nm in a folded capillary polycarbonate cell with gold

electrodes. The potential applied between the electrodes was set around 150 V. The measurements were performed in triplicate at 25°C on a dilute DW_0 aqueous suspension (~ 2 $mg.L^{-1}$). Small amounts of a 0.1 $mol.L^{-1}$ NaOH solution were added stepwise ($\Delta pH \sim 0.5$) under stirring and, after an equilibrium time of 1 min, the electrophoretic mobility was determined as a function of pH.

Samples preparation by osmotic stress. Osmotic stress (here, dialysis against a polymer solution) is a convenient way to obtain concentrated suspensions of colloidal charged particles,[54] and has been widely employed to explore the phase diagram of clay nanosheets.[10,12,14,16] Maillet showed that concentrated suspensions of aluminogermanate single-walled imogolite nanotubes can also be prepared by osmotic compression using Dextran; however control of electrostatic interactions had not been undertaken.[55] To achieve this goal, batches of suspensions were prepared from the initial stock of DW_0 suspension at a fixed ionic strength (IS = 10^{-4} – 1 $mol.L^{-1}$).[14] Typically, dialysis membranes (Spectra/Por, cut-off 10 kDa, Spectrum) were filled with stock suspension and placed in a 1 L reservoir of PEG_{20000} solution prepared by dilution with the appropriate amount of NaCl. Under such conditions, the ionic strength is fixed in the reservoir, which avoids problems related with the Donnan effect.[56] The osmotic pressure was imposed during two weeks to obtain concentrated suspensions. The Ge-DWINTs suspensions were then recovered and the volume fraction ϕ was determined as:

$$\phi = \frac{C}{\rho_{vol}} \qquad (2)$$

with C being the solid concentration of Ge-DWINTs determined by weight loss upon drying, taking into account the weight of residual NaCl, especially at high ionic strength. ρ_{vol} is the density of a Ge-INT (3.64 $g.cm^{-3}$). For each IS value, series of samples have been prepared by dilution with NaCl solution at constant ionic strength to scan the ϕ/IS phase diagram.

X-ray scattering measurements. Selected samples of Ge-DWINTs suspensions were held in borosilicate capillary tubes (WJM-Glas/Müller GmbH, DE) of 1 mm diameter and stored vertically after flame-sealing. Wide-Angle X-ray Scattering (WAXS) experiments were carried out on a Cu rotating anode (RU H3R, Rigaku Corporation, Japan) at a wavelength of $\lambda_{CuK\alpha}$ = 0.1542 nm delivered by a multilayer W/Si mirror (Osmic). Two-dimensional (2D) WAXS patterns were collected on a MAR345 detector (marXperts GmbH, Germany) with 150 µm pixel size, placed at a sample-to-detector distance of 300 mm. The experimental resolution can be approximated by a Gaussian with Full-Width at Half Maximum (FWHM) ~0.13 nm^{-1}. Small-Angle X-ray Scattering (SAXS) experiments were carried out at the TRUSAXS ID02 beamline of the synchrotron ESRF (Grenoble, France) at a wavelength of λ = 0.095 nm.[57] 2D SAXS patterns were acquired on a FReLoN (Fast-Readout Low-Noise) camera with 52.5 µm pixel size and placed in a vacuum detection tunnel at a sample to detector distance of 2 m.

In both cases, the intensity versus scattering vector modulus Q ($Q = 4\pi/\lambda \sin(\theta)$, where λ is the incident wavelength and 2θ is the scattering angle) curves were deduced from the azimuthal angular integration [0, 2π] of the scattering patterns, previously corrected for water and glass scattering using homemade software.

RESULTS AND DISCUSSION

Characterization of initial stock (DW_0) colloid sample. INTs are easily obtained by sol-gel methods. However, both the morphology and the surface properties of INTs strongly depend on the synthesis route used.[30,49,58] We first characterized the initial stock of dialyzed DW_0 by using transmission electron microscopy (TEM) observations. A representative TEM micrograph is presented in Figure 2a, evidencing well-dispersed individual nanotubes. The nanotube length

(NLD) and diameter distributions (NDD), deduced from the analysis of more than 500 nanotubes, are plotted as histograms in Figure 2b,c and the deduced morphological parameters are summarized in Table 1. The NLD follows a log-normal distribution with a mean length $\langle L \rangle$ = 18 ± 1.6 nm but with a relatively high PDI_L value (Table 1), as expected for INTs samples synthesized in similar conditions.[44,52] By contrast, the NDD remains highly monodisperse (PDI_D = 7%) with a normally distributed diameter centered at $\langle D \rangle$ = 4.3 ± 0.3 nm, in close agreement with previous results obtained from X-ray scattering experiments.[44] Accordingly, the aspect ratio $\langle L \rangle / \langle D \rangle$ of these nanotubes remains extremely low (Table 1), showing that they represent an attractive model of nanotubes with well-defined morphology.

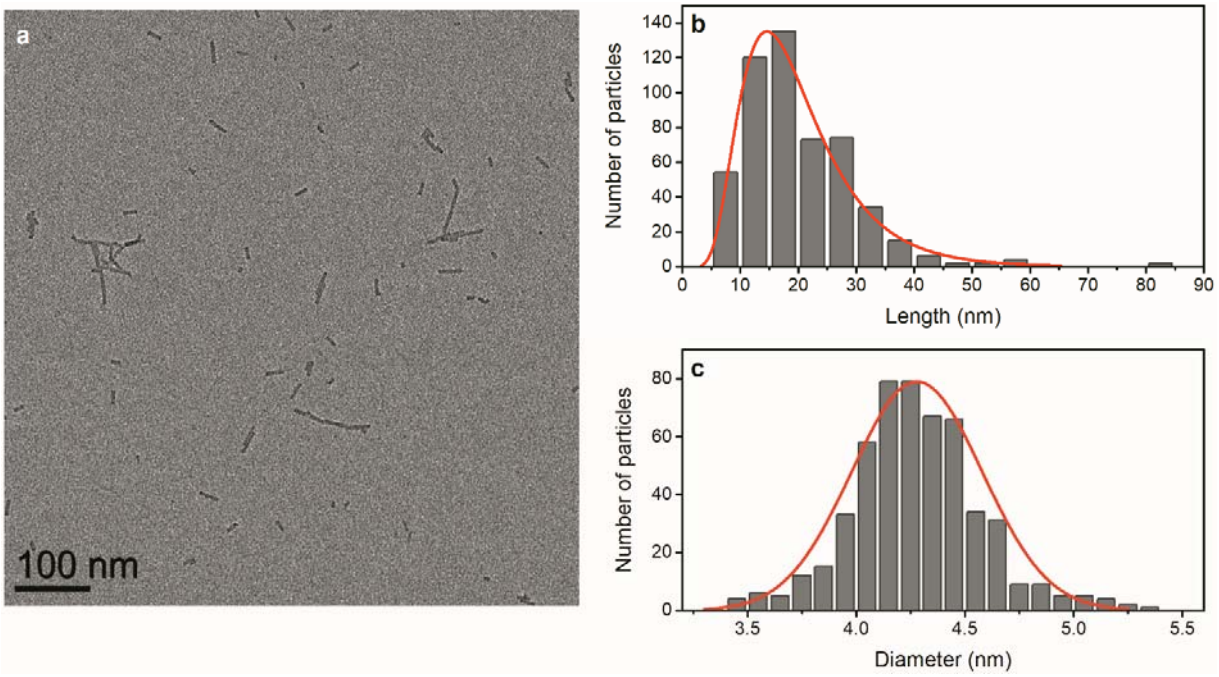

Figure 2. (a) Typical TEM micrograph of individually nanotubes obtained from a dilute suspension of DW_0. Histograms of the (b) nanotube length distribution NLD (red curve: log-normal fitting) and (c) nanotube diameter distribution NDD (red curve: Gaussian fitting).

Table 1. Morphological parameters deduced from the analysis of the TEM micrographs.

$\langle L \rangle$ (nm)	PDI_L (%)	$\langle D \rangle$ (nm)	PDI_D (%)	Aspect ratio
18.0 ± 1.6	49	4.3 ± 0.3	7	4.2

Figure 3a presents the IR spectrum obtained on the 1300-400 cm^{-1} range, an area related to the INT backbone. The band at 915 cm^{-1} and the doublet at 825 and 805 cm^{-1} are specific to Ge-O stretching vibrations for well-formed tubular structures.[42,44,59] Below, we find a large absorption band, typical of the imogolite-like local structure.[42,60] The bands located at 690 and 555 cm^{-1} are assigned to Al-O stretching vibrations arising from the INT structure, while the peaks at 465 and 420 cm^{-1} seem to be related to various –OH, Ge-O-Al and Ge-O bending modes.[42,60] In addition, the band between 1200 and 1100 cm^{-1} corresponds to residual perchlorates anions adsorbed on the outside surfaces of DW_0.

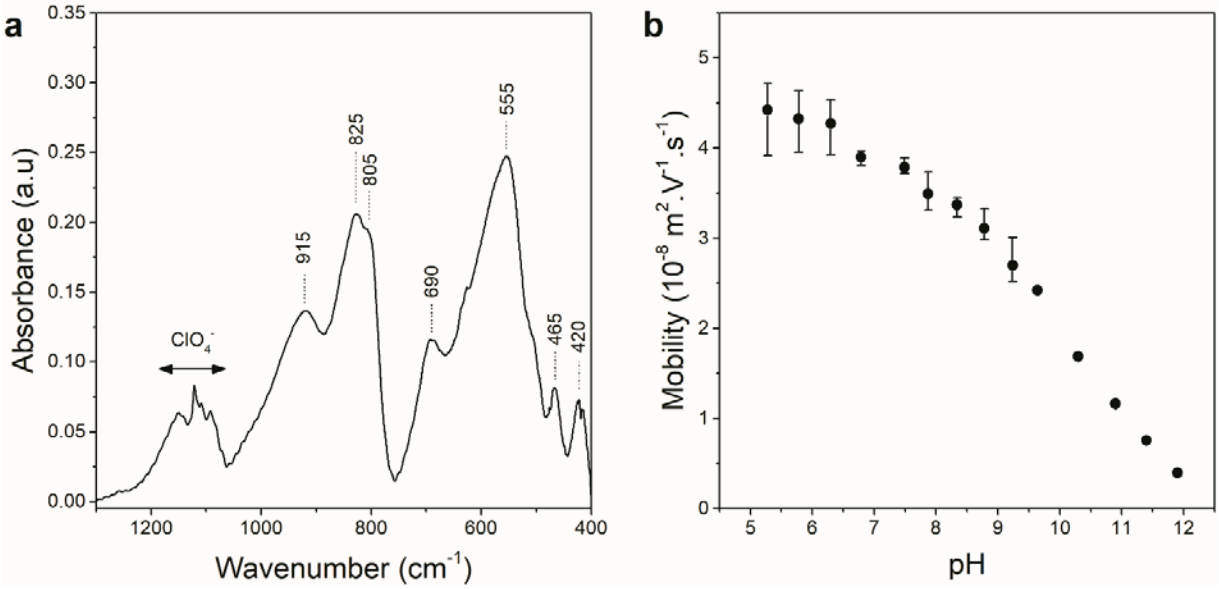

Figure 3. (a) Infrared spectrum obtained on a powder of DW_0. (b) Evolution of the electrophoretic mobility as a function of the pH on a dilute suspension of DW_0.

Since the surface charge of INTs seems to be at the origin of the nanotube affinity to ion adsorption,[45] this property was assessed by performing electrokinetic measurements on a dilute

DW_0 sample (see Method section) to reduce the probability of double-layer interaction. Figure 3b presents the evolution of the electrophoretic mobility as a function of the pH. The DW_0 suspension displays a positive mobility μ in the whole range of pH studied. The value of μ is fairly constant around 4.5 10^{-8} $m^2.V^{-1}.s^{-1}$ for pH ≤ 6, indicating saturated protonation of the nanotube outer surface ($–AlOH_2^+$ groups)[45,61] for such pH values. Then it decreases almost linearly with pH similarly as observed previously for single-walled aluminosilicate[41,62,63] and aluminogermanate nanotubes.[42] Interestingly, the use of the isoelectrical point (IEP), i.e. the pH at which the electrophoretic mobility is zero, has been proposed as an alternative method to evaluate the formation of INTs.[64] The increase of IEP to alkaline values seems to reflect a decrease of the contribution of both terminal ≡Al-OH and ≡Ge-OH groups on the INT surface charge.[64]. In the present work, the –Al-OH groups remain protonated over a wide range of pH with an IEP value around 12, more than two orders of magnitude higher than the IEP value reported for Ge-SWINTs.[42] Although the latter form much longer nanotubes (lower contribution of tube-ends on the electrophoretic mobility),[31] this result thus suggests that, even if the DW_0 sample has low aspect ratio (Table 1), it is made of well-formed INTs with a low ratio of edge defects.

Phase diagram. Starting from the initial stock of DW_0, concentrated Ge-DWINTs suspensions were prepared at different ionic strengths (IS = 10^{-4}, 10^{-3}, 10^{-2}, 10^{-1} and 1 $mol.L^{-1}$) to scan the ϕ/IS phase diagram. These suspensions were transferred in glass vials for naked-eye optical observations, either in natural light (Figure 4) or between crossed polarizers (Figure S1). At high ionic strengths (IS ≥ 10^{-1} $mol.L^{-1}$), the predominance of attractive van der Waals interactions induces the aggregation of INTs. All samples form opaque aggregates that slowly settle down after few days, the proportion of sediment increasing with the volume fraction (Figure 4a,b). When the volume fraction ϕ reaches values higher than 1.5%, these aggregates no longer sediment but form

instead an arrested (attractive gel) phase (Figure S2). In contrast, a clear change appears at lower ionic strength. Indeed, all samples display stable transparent colloidal dispersions over a wide range of volume fractions (Figure 4c-e). Whatever the IS value (10^{-4}-10^{-2} mol.L^{-1}), the viscosity gradually increases with ϕ and, above a certain volume fraction, the dispersions form instantaneously a gel phase (Figure 4d,e),[40,65] which remains completely transparent. These gel phases become birefringent for $\phi > 1\%$ (Figure S1), meaning that Ge-DWINTs are "frozen" with preferred orientations.

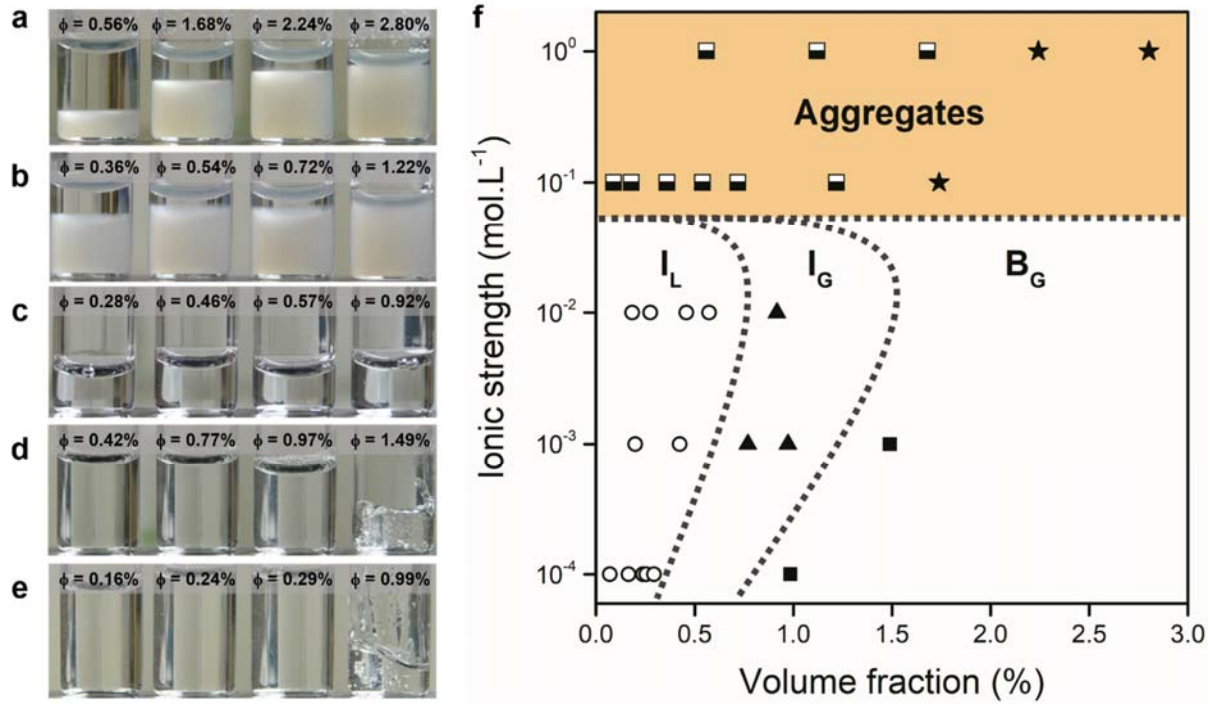

Figure 4. (a-e) Optical observations of aqueous suspensions of Ge-DWINT prepared at different ionic strengths, as a function of the volume fraction ϕ. (a) IS = 1 mol.L^{-1}; (b) IS = 10^{-1} mol.L^{-1}; (c) IS = 10^{-2} mol.L^{-1}; (d) IS = 10^{-3} mol.L^{-1}; (e) IS = 10^{-4} mol.L^{-1}. (f) Corresponding phase diagram as a function of Ge-DWINT volume fraction ϕ and ionic strength. The dotted lines between the different regimes are only eye guide. I_L (open circles): isotropic liquid; I_G (black triangles):

isotropic gel; B_G (black squares): birefringent gel; Squares with bottom half black symbolize suspensions forming opaque sediments while stars indicate attractive gels.

From these macroscopic optical observations, we were able to establish the first phase diagram representing the effect of ionic strength as a function of the volume fraction in aqueous suspensions of Ge-DWINT (Figure 4f). As stated in the introduction, the colloidal stability of charged nanoparticles like Ge-DWINTs can be divided, in principle, into two domains controlled by the ionic strength of the medium. At low ionic strength, the Debye screening length κ^{-1} of the diffuse double layer is large (e.g. $\kappa^{-1} = 0.304/\sqrt{IS}$ = 30.4 nm for IS = 10^{-4} mol.L^{-1}), inducing the stabilization of nanotubes by electrostatic repulsions. The liquid/gel transition also displays a positive slope, which hints at the repulsive nature of the interactions.[14,66] At higher ionic strength, the Debye length is strongly reduced. Abend & Lagaly have clearly demonstrated that the interactions between clay nanosheets particles become attractive at a ionic strength of about 0.01 mol.L^{-1} (also referred as the critical coagulation concentration).[9] Similar behavior was also observed in colloidal dispersions of boehmite rods.[61] We observe the same effect here since coagulation of Ge-DWINTs starts to occur above this critical concentration, where κ^{-1} is of the same order of magnitude as the diameter of Ge-DWINTs. Finally, it can be pointed out that the general appearance of this phase diagram for 1D charge nanoparticles is in good agreement with those reported for 2D charged layered materials such as swelling clays,[9,10,12,14] layered double hydroxide,[67] or takovites.[68]

Nanotubes local organization. The transition from repulsive to attractive interactions should affect the local structural organization of Ge-DWINTs. We investigate this effect by first carrying out WAXS experiments on the most concentrated samples obtained at each IS value (Figure 5a).

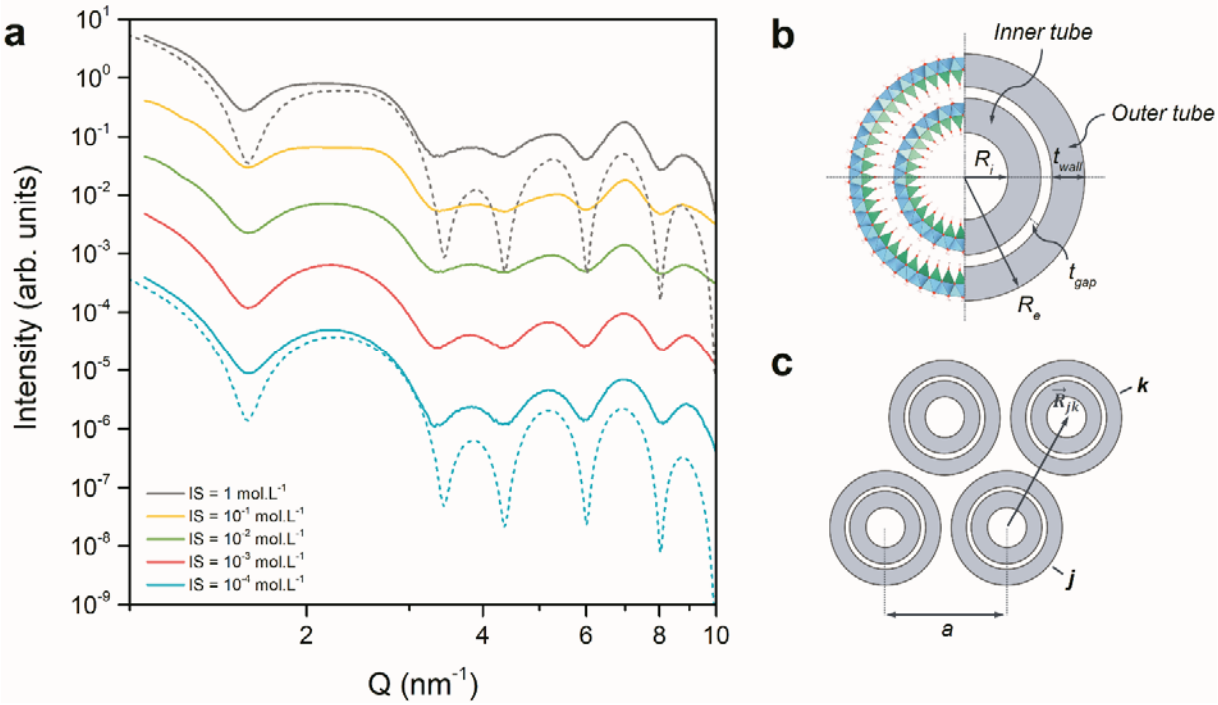

Figure 5. (a) Evolution of WAXS diagrams of Ge-DWINTs suspensions upon increasing the ionic strength: IS = 10^{-4} mol.L^{-1} (ϕ = 0.99%); IS = 10^{-3} mol.L^{-1} (ϕ = 1.49%); IS = 10^{-2} mol.L^{-1} (ϕ = 0.92%); IS = 10^{-1} mol.L^{-1} (ϕ = 1.74%); IS = 1 mol.L^{-1} (ϕ = 2.80%). Dotted lines correspond to calculated WAXS diagrams using eq. 3 (see text for details): (blue) DW_1^{sim} ($N_b = 1, p = 1$); (grey) DW_{1-3}^{sim} (a = 4.5 nm, N_b = 1, p = 0.3; N_b = 2, p = 0.6; N_b = 3, p = 0.1). All curves have been translated vertically for the sake of clarity. (b) Schematic representation in the homogeneous approximation of a Ge-DWINT nanotube perpendicular to its long axis. (c) Sketch of a bundle of four Ge-DWINTs in a hexagonal close packing of lattice parameter a.

All WAXS diagrams exhibit the expected intensity modulations characteristic of a double-walled nanotube in the 4-10 nm^{-1} Q-range,[25] which are related to the interferences between inner and outer tubes.[69] Beyond this proof of the DW structure, the most striking feature is probably the stepwise flattening of the first oscillation centered at Q = 2.2 nm^{-1} along with a shape modification of the subsequent oscillations, in particular at Q = 5 nm^{-1}, for IS $\geq$ 10^{-2} mol.L^{-1} (Figure 5a).

However, the WAXS diagrams do not exhibit any narrow Bragg peaks, suggesting that the local structural organization, if any, is rather restricted to bundles with limited size.[42] X-ray scattering diagrams can be used to reveal accurate information on both morphology and spatial organization of imogolite-like nanotubes.[25,27,42] For small scattering wave-vectors (Q < 10 nm^{-1}), WAXS diagrams can be fitted within the homogenous approximation. In the present case, Ge-DWINT is modelled by two hollow cylinders with equal wall thickness t_{wall}, a distance t_{gap} in between and electronic density ρ_{INT} (0.91 e$^-$.Å^{-3}) as schematized in Figure 5b. The Ge-DWINT is defined by its external radius $R_e = R_i + 2t_{wall} + t_{gap}$ with R_i the inner radius of the inner tube and t_{gap} the gap thickness between the inner and outer tubes. For the sake of clarity, we consider nanotubes with infinite length in the calculation of WAXS diagrams. For interested readers, a complete description of the X-ray formalism used to fit the WAXS data of nanotubes can be found elsewhere.[70,71] Briefly, the scattered intensity from Ge-DWINTs of infinite length, with random orientations, is simply the product of the squared form factor $P(Q)$ of the nanotube by the structure factor $S(Q)$ of the bundle, renormalized to the wave-vector:

$$I(Q) \propto \frac{1}{Q} P(Q)^2 S(Q) \tag{3}$$

where $P(Q)$ and $S(Q)$ are defined as:

$$P(Q) = \left(\rho_{\mathrm{INT}} f_{\mathrm{INT}}(Q) - \rho_{\mathrm{w}} f_{\mathrm{w}}(Q)\right)\left(F_{R_{\mathrm{e}}} - F_{R_{\mathrm{e}}-t_{\mathrm{wall}}} + F_{R_{\mathrm{i}}+t_{\mathrm{wall}}} - F_{R_{\mathrm{i}}}\right) \tag{4a}$$

$$S(Q) = \sum_{N_{\mathrm{b}}} p_{N_{\mathrm{b}}} \sum_{jk} J_0\left(Q R_{jk}\right) \tag{4b}$$

with f_{INT} and f_w the normalized X-ray scattering factor of an imogolite unit and a water molecule, respectively; ρ_w (0.334 e$^-$.Å^{-3}) is the electronic density of water inside and outside the nanotubes, F_R is the Fourrier transform of the projection of a full cylinder of radius R along its axis.The term p_{N_b} yields the proportion of each type of bundle formed by N_b nanotubes in the sample while R_{jk}

is the modulus of the vector joining the centers of tubes *j* and *k* in a bundle, in the plane perpendicular to its axis (Figure 5c). We chose as a first approximation a hexagonal packing configuration with a lattice parameter *a*, which is ultimately the structure adopted by nanotubes in large bundles.[25,42]

Experimental WAXS diagrams obtained at IS = 10^{-4} mol.L^{-1} are well reproduced considering dispersions of individual nanotubes ($N_b = 1$, $p = 1$) with $R_i = 0.77$ nm, $t_{wall} = 0.58$ nm and $t_{gap} = 0.2$ nm (blue dotted curve in Figure 5a), the calculated $2R_e = 4.26$ nm being in close agreement to the $\langle D \rangle$ value determined from TEM measurements (Table 1). It must also be emphasized that the transition from an isotropic liquid (I_L, $\phi = 0.26\%$) to a birefringent gel phase (B_G, $\phi = 0.99\%$) does not modify the WAXS diagram (Figure S3), implying in both cases the presence of individual nanotubes only. Similar behaviors are also observed for samples prepared at IS = 10^{-3} mol.L^{-1} (Figure 5a), which confirm the predominance of repulsive interactions between Ge-DWINTs in this range of IS values, in agreement with optical observations (Figure 4). For IS $\geq 10^{-2}$ mol.L^{-1}, the WAXS curves no longer match obviously the scattering diagram of individual nanotubes. A structure factor needs to be taken into consideration in eq. (3) to account for experimental data. We first explored different scenarios of bundling, varying both the number of tubes per bundle and the lattice parameter *a* (Figure S4). The slight deformation of the oscillations coupled with the lack of Bragg peaks indicate the presence of small bundles, containing only a few tubes. However, the presence of only one population of bundles (N_b fixed) can be ruled out since the simulated WAXS diagrams do not allow to reproduce the deformation of the scattered intensity. Instead, a *qualitative* fit is obtained considering a mixture of bundles ($N_b < 4$) with a mean lattice parameter $a = 4.5$ nm , corresponding to a 2 Å gap between the nanotubes (Figure 5a). Such a value is reasonable if one considers intertube interactions and the possible presence of anions bounded on the outer surface

of the nanotubes. It can be pointed out that errors on the proportion of each type of bundle are relatively significant due to the relative limited size of the bundles as evidenced for Ge-SWINTs,[42] and similar WAXS diagrams may be obtained by slightly altering p_{N_b} values (Figure S4d). Nevertheless, our results clearly show that the formation of bundles in aqueous suspensions is related to a reduction of the electrostatic interactions by a screening effect of the nanotube surface charge via the condensation of anions, most probably on the outer surface of Ge-DWINTs.[45]

Structure of the suspensions and swelling law. To get a more general overview of the colloidal properties of Ge-DWINTs, their structural organization at larger distances was assessed from SAXS experiments in the different domains of the phase diagram. Starting from the lowest ionic strength and up to 10^{-2} mol.L^{-1}, SAXS curves present similar decay as the calculated diagram for dispersions of individual nanotubes DW_1^{sim} ($N_b = 1$, $p = 1$) (Figure 6). The decay of the scattered intensity I with scattering vector modulus Q follows a Q^{-1} dependence, related to the one-dimensional particle form factor $P(Q)$ of the scattered INTs described in eqs. (3) and (4a). It means therefore that these samples are formed of individual nanotubes, regardless the colloidal state of the system (I_L, I_G or B_G) or the volume fraction. In contrast, the slope of the SAXS curves systematically evolves to a -2 exponent when the ionic strength rises above IS $\geq 10^{-1}$ mol.L^{-1} (Figure 6). We have seen that Ge-DWINTs are no longer organized individually but are stacked locally in small bundles forming micrometer-sized aggregates of Ge-DWINTs, as evidence from optical observations (Figure 4a,b). Assuming a similar behavior as the one reported for 2D swelling clays,[19] the appearance of this Q^{-2} slope can be reasonably interpreted as resulting from the formation of these aggregates, due to the onset of dominating attractive interactions.

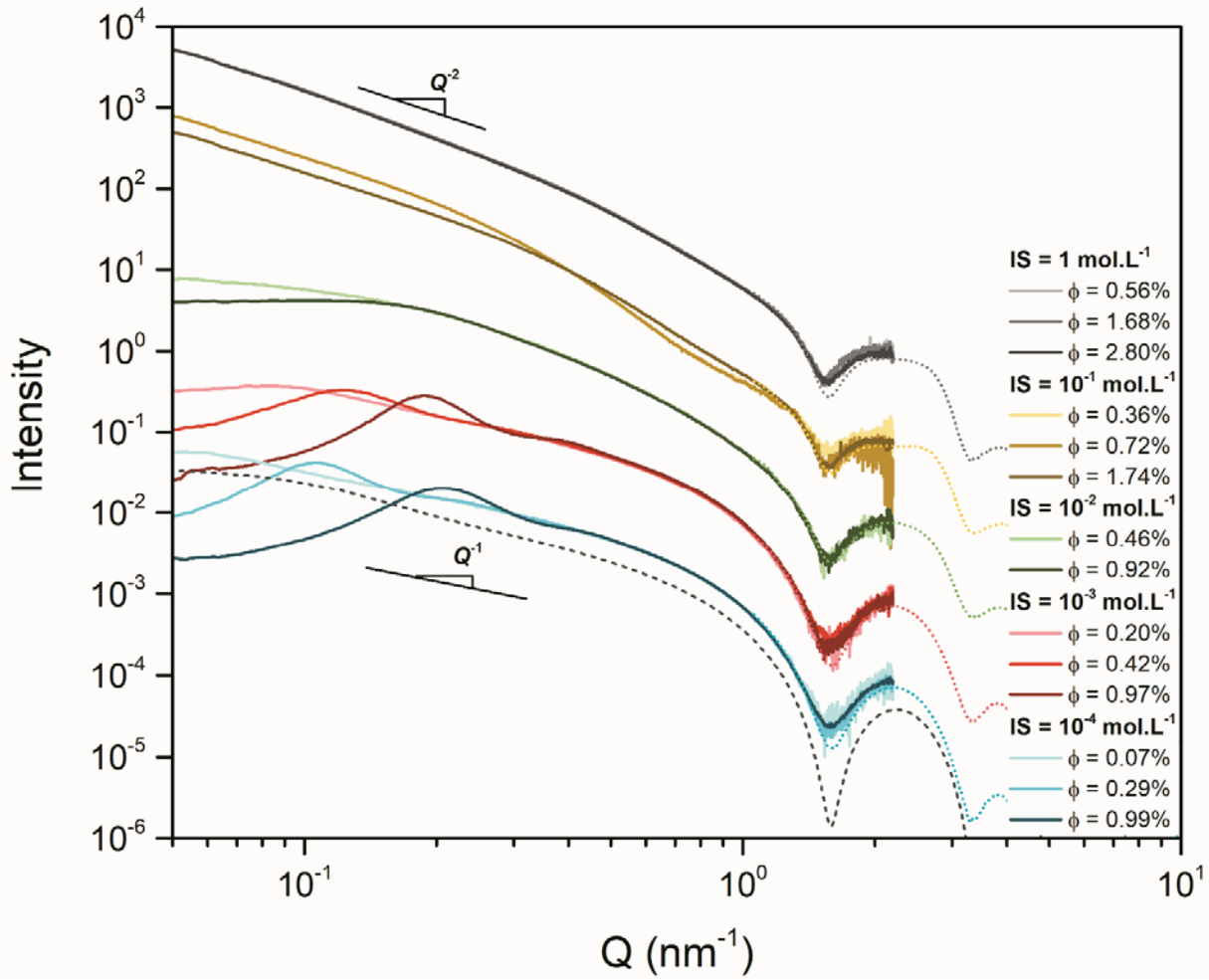

Figure 6. Variation of the SAXS diagrams of Ge-DWINTs suspensions upon increasing the ionic strength: IS = 10^{-4} mol.L^{-1} (blue); IS = 10^{-3} mol.L^{-1} (red); IS = 10^{-2} mol.L^{-1} (green); IS = 10^{-1} mol.L^{-1} (yellow); IS = 1 mol.L^{-1} (grey). Dotted lines correspond to WAXS curves obtained for the most concentrated samples at each IS value. Dashed line corresponds to calculated WAXS diagram using eq. 3 for individual Ge-DWINTs (DW_1^{sim}, N_b = 1, p = 1). All curves have been translated for the sake of clarity.

Beyond the evolution of the slope of the $I(Q)$ curves, a modulation of the scattered intensity is also observed in the low Q region of the SAXS curves for IS ≤ 10^{-2} mol.L^{-1}. Its position depends on the volume fraction, shifting to lower Q values (larger distances) with decreasing the

concentration of Ge-DWINTs. Modulations are due to short-range positional order of the nanotubes over large distances in the plane perpendicular to their main axis,[25] either in the isotropic liquid (I_L) or in the gel phases I_G & B_G of the phase diagram (Figure 6). The average interparticle distance *d* can be deduced from the position of the first maximum as:

$$d = \frac{2\pi}{Q_{max}} \tag{5}$$

By using eq. 5, the evolution of the average interparticle distance as a function of the volume fraction, the so-called swelling (or dilution) law, can be obtained. Assuming a local hexagonal configuration of the nanotubes as the packing limit that nanotubes can reach,[25,42] the relation between *d* and volume fraction in the case of 1D particles is of the form:[72,73]

$$d = \left(\pi\sqrt{3}/8\right)^{1/2}\langle D\rangle\phi^{-0.5} \tag{6}$$

with $\langle D\rangle$ being the mean diameter of the nanotube. Despite the limited range of the volume fraction we investigated, dispersions of Ge-DWINTs seem to follow such swelling law related to a two-dimensional swelling for the most concentrated samples (Figure 7).

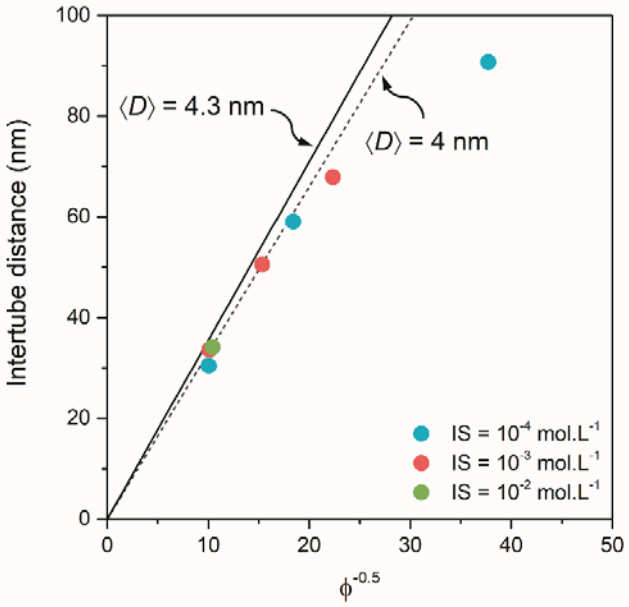

Figure 7. Evolution of the interparticle distance obtained from the SAXS curves as a function of $\phi^{-0.5}$ and for different ionic strength. The two black curves correspond to linear fit using eq. 6 (see text for details).

Similar evolution has already been observed for aqueous dispersions of aluminosilicate and aluminogermanate single-walled imogolite nanotubes.[55,74] It is also worth noting that the interparticle distances deviate from linearity due to the predominance of isotropic swelling occurring at low volume fractions ($\phi^{-0.5} \geq 20$). As shown from eq. 6, the slope of the swelling law should be used to derive the average diameter $\langle D \rangle$ of Ge-DWINTs. In our case, the obtained value is close to 4 nm, in agreement with the diameter of individual nanotubes derived either from TEM measurements (Table 1) or WAXS simulations (Figure 5a). It should be noted that the so-called percolation threshold ϕ_t of homogeneous gels of one-dimensional objects writes:[40]

$$\phi_{gel} \frac{L}{D} > 0.7 \quad (7)$$

Here, the minimum value of ϕ_{gel} is found to be around 0.5% for nanotubes with aspect ratio of 4.2, leading to a value $\phi_{gel} \frac{L}{D} \approx 0.02$ significantly lower than 0.7. The gelation of our colloidal Ge-DWINTs at low ionic strength is related to a complex situation due to the interplay between electrostatic interactions, translational and rotational Brownian motion and orientation phenomena rather than a long-range connectivity between the nanotubes. For IS $\geq 10^{-2}$ mol.L^{-1}, X-ray scattering and optical results reveal the existence of small bundles arranged in structures much larger than the size of individual nanotubes. From a fundamental point of view, it would certainly be relevant to assess the correlation length in these aggregated structures, a tricky investigation that goes beyond the purpose of this study.

CONCLUSIONS

In summary, we unravel the colloidal stability of double-walled aluminogermanate imogolite nanotubes. By carefully controlling both ionic strength of the medium and the volume fraction in nanotubes, we were able to propose a complete phase diagram from the combination of optical observations and SAXS/WAXS experiments. Although the overall topology of the phase diagram is similar to that of clay nanosheets, the position of the different phase boundary are different, which may be related to the difference in electrostatic double-layer interaction energy between clay minerals with differing geometries and aspect ratio.[75] In the repulsive regime, i.e. at IS < 10^{-2} $mol.L^{-1}$, Ge-DWINTs are dispersed individually in aqueous suspensions and form stable, isotropic sol. These transparent suspensions turn out as a gel phase over a critical volume fraction threshold, whose position shifts to higher concentration when the ionic strength increases. In all cases, Ge-DWINTs behave like "swelling" clay nanosheets, the average interparticle distance following the inverse square root of the nanotube volume fraction. Above IS ≥ 10^{-2} $mol.L^{-1}$, the Debye screening length is not sufficient to prevent nanotubes from coagulation. As a result, Ge-DWINTs are stacked together in bundles with a hexagonal close-packing configuration, forming aggregates, which collapse under gravity or form opaque (attractive) arrested phases depending on the nanotube concentration. Altogether, these results provide a basis for the colloidal stability of imogolite-like nanotubes, which could open new pathways for designing hydrogels,[34] nanocomposites,[76] or membranes,[77] based on these geo-inspired INTs. Beyond applications, imogolite nanotubes are singular since their surface is highly curved, which in turn complicate the analytical calculation of electrostatic double-layer interaction energies. Here, we demonstrated that Ge-DWINTs can be considered as a model charged nanotube due to their well-defined diameter, high colloidal stability while controlling their aspect ratio by soft chemistry.[25,44] Therefore, it

would certainly be relevant to use them for investigating in depth the energy of interaction depending onthe separation distance, ionic strength and valence of the counterions, a pending issue for charged nanocylinders.

ASSOCIATED CONTENT

Supporting Information. The following files are available free of charge.

Additional optical observations of aqueous suspensions between crossed polarizers and WAXS diagrams simulations (PDF)

AUTHOR INFORMATION

Corresponding Author

*E-mail: erwan-nicolas.paineau@u-psud.fr. Phone: +33 (0) 1 69 15 60 51.

Notes

The authors declare no competing financial interest.

ACKNOWLEDGMENT

The present work has benefited from the Electronic Microscopy facility of Imagerie-Gif, (http://www.i2bc.paris-saclay.fr), member of IBiSA (http://www.ibisa.net), supported by "France-BioImaging" (ANR-10-INBS-04-01), and the Labex "Saclay Plant Science" (ANR-11-IDEX-0003-02). E.P. would like to thank Dr. P. Davidson for access to ID02 experiments (ESRF, proposal SC4867) and Dr. Lewis Sharpnack for his help during SAXS experiments.

REFERENCES

(1) Duncan, T. V. Applications of Nanotechnology in Food Packaging and Food Safety: Barrier Materials, Antimicrobials and Sensors. *J. Colloid Interface Sci.* **2011**, *363*, 1–24.
(2) Zhou, D.; Abdel-Fattah, A. I.; Keller, A. A. Clay Particles Destabilize Engineered Nanoparticles in Aqueous Environments. *Environ. Sci. Technol.* **2012**, *46*, 7520–7526.
(3) Swartzen-Allen, S. L.; Matijevic, E. Surface and Colloid Chemistry of Clays. *Chem. Rev.* **1974**, *74*, 385–400.
(4) Lagaly, G. Colloid Clay Science. In *Developments in Clay Science*; Elsevier, **2006**; Vol. 1, pp 141–245.
(5) Langmuir, I. The Role of Attractive and Repulsive Forces in the Formation of Tactoids, Thixotropic Gels, Protein Crystals and Coacervates. *J. Chem. Phys.* **1938**, *6*, 873–896.
(6) Norrish, K. The Swelling of Montmorillonite. *Discuss. Faraday Soc.* **1954**, *18*, 120–134.
(7) Ramsay, J. D. F. Colloidal Properties of Synthetic Hectorite Clay Dispersions: I. Rheology. *J. Colloid Interface Sci.* **1986**, *109*, 441–447.
(8) Mourchid, A.; Lecolier, E.; Van Damme, H.; Levitz, P. On Viscoelastic, Birefringent, and Swelling Properties of Laponite Clay Suspensions: Revisited Phase Diagram. *Langmuir* **1998**, *14*, 4718–4723.
(9) Abend, S.; Lagaly, G. Sol–gel Transitions of Sodium Montmorillonite Dispersions. *Appl. Clay Sci.* **2000**, *16*, 201–227.
(10) Michot, L. J.; Bihannic, I.; Porsch, K.; Maddi, S.; Baravian, C.; Mougel, J.; Levitz, P. Phase Diagrams of Wyoming Na-Montmorillonite Clay. Influence of Particle Anisotropy. *Langmuir* **2004**, *20*, 10829–10837.
(11) Tombacz, E.; Szekeres, M. Colloidal Behavior of Aqueous Montmorillonite Suspensions: The Specific Role of PH in the Presence of Indifferent Electrolytes. *Appl. Clay Sci.* **2004**, *27*, 75–94.
(12) Michot, L. J.; Bihannic, I.; Maddi, S.; Funari, S. S.; Baravian, C.; Levitz, P.; Davidson, P. Liquid–crystalline Aqueous Clay Suspensions. *Proc. Natl. Acad. Sci.* **2006**, *103*, 16101–16104.
(13) Ruzicka, B.; Zulian, L.; Ruocco, G. More on the Phase Diagram of Laponite. *Langmuir* **2006**, *22*, 1106–1111.
(14) Paineau, E.; Antonova, K.; Baravian, C.; Bihannic, I.; Davidson, P.; Dozov, I.; Imperor-Clerc, M.; Levitz, P.; Madsen, A.; Meneau, F.; Michot, L. J. Liquid-Crystalline Nematic Phase in Aqueous Suspensions of a Disk-Shaped Natural Beidellite Clay. *J. Phys. Chem. B* **2009**, *113*, 15858–15869.
(15) Lagaly, G.; Ziesmer, S. Colloid Chemistry of Clay Minerals: The Coagulation of Montmorillonite Dispersions. *Adv. Colloid Interface Sci.* **2003**, *100*, 105–128.
(16) Paineau, E.; Bihannic, I.; Baravian, C.; Philippe, A.-M.; Davidson, P.; Levitz, P.; Funari, S. S.; Rochas, C.; Michot, L. J. Aqueous Suspensions of Natural Swelling Clay Minerals. 1. Structure and Electrostatic Interactions. *Langmuir* **2011**, *27*, 5562–5573.
(17) Ruzicka, B.; Zaccarelli, E.; Zulian, L.; Angelini, R.; Sztucki, M.; Moussaïd, A.; Narayanan, T.; Sciortino, F. Observation of Empty Liquids and Equilibrium Gels in a Colloidal Clay. *Nat. Mater.* **2011**, *10*, 56.
(18) Paineau, E.; Philippe, A. M.; Antonova, K.; Bihannic, I.; Davidson, P.; Dozov, I.; Gabriel, J. C. P.; Imperor-Clerc, M.; Levitz, P.; Meneau, F.; Michot, L. J. Liquid-Crystalline Properties of Aqueous Suspensions of Natural Clay Nanosheets. *Liq. Cryst. Rev.* **2013**, *1*, 110–126.

(19) Michot, L. J.; Bihannic, I.; Thomas, F.; Lartiges, B. S.; Waldvogel, Y.; Caillet, C.; Thieme, J.; Funari, S. S.; Levitz, P. Coagulation of Na-Montmorillonite by Inorganic Cations at Neutral PH. A Combined Transmission X-Ray Microscopy, Small Angle and Wide Angle X-Ray Scattering Study. *Langmuir* **2013**, *29*, 3500–3510.
(20) Rosenfeldt, S.; Stöter, M.; Schlenk, M.; Martin, T.; Albuquerque, R. Q.; Förster, S.; Breu, J. In-Depth Insights into the Key Steps of Delamination of Charged 2D Nanomaterials. *Langmuir* **2016**, *32*, 10582–10588.
(21) Woolston, P.; van Duijneveldt, J. S. Isotropic–nematic Phase Transition in Aqueous Sepiolite Suspensions. *J. Colloid Interface Sci.* **2015**, *437*, 65–70.
(22) Lisuzzo, L.; Cavallaro, G.; Parisi, F.; Milioto, S.; Lazzara, G. Colloidal Stability of Halloysite Clay Nanotubes. *Ceram. Int.* **2019**, *45*, 2858–2865.
(23) Woolston, P.; van Duijneveldt, J. S. Isotropic-Nematic Phase Transition in Aqueous Sepiolite Suspensions. *J. Colloid Interface Sci.* **2015**, *437*, 65–70.
(24) Luo, Z.; Song, H.; Feng, X.; Run, M.; Cui, H.; Wu, L.; Gao, J.; Wang, Z. Liquid Crystalline Phase Behavior and Sol–gel Transition in Aqueous Halloysite Nanotube Dispersions. *Langmuir* **2013**, *29*, 12358–12366.
(25) Paineau, E.; Krapf, M.-E. M.; Amara, M.-S.; Matskova, N. V.; Dozov, I.; Rouziere, S.; Thill, A.; Launois, P.; Davidson, P. A Liquid-Crystalline Hexagonal Columnar Phase in Highly-Dilute Suspensions of Imogolite Nanotubes. *Nat. Commun.* **2016**, *7*, 10271.
(26) Cradwick, P. D. G.; Wada, K.; Russell, J.; Yoshinaga, N.; Masson, C.; Farmer, V. Imogolite, a Hydrated Aluminum Silicate of Tubular Structure. *Nat.-Phys. Sci.* **1972**, *240*, 187–189.
(27) Monet, G.; Amara, M. S.; Rouzière, S.; Paineau, E.; Chai, Z.; Elliott, J. D.; Poli, E.; Liu, L.-M.; Teobaldi, G.; Launois, P. Structural Resolution of Inorganic Nanotubes with Complex Stoichiometry. *Nat. Commun.* **2018**, *9*, 2033.
(28) Nanzyo, M.; Kanno, H. Non-Crystalline Inorganic Constituents of Soil. In *Inorganic Constituents in Soil*; Springer, 2018; pp 59–95.
(29) Farmer, V.; Fraser, A.; Tait, J. Synthesis of Imogolite - Tubular Aluminum Silicate Polymer. *J. Chem. Soc.-Chem. Commun.* **1977**, *13*, 462–463.
(30) Yucelen, G. I.; Kang, D.-Y.; Guerrero-Ferreira, R. C.; Wright, E. R.; Beckham, H. W.; Nair, S. Shaping Single-Walled Metal Oxide Nanotubes from Precursors of Controlled Curvature. *Nano Lett.* **2012**, *12*, 827–832.
(31) Amara, M. S.; Paineau, E.; Rouziere, S.; Guiose, B.; Krapf, M.-E. M.; Tache, O.; Launois, P.; Thill, A. Hybrid, Tunable-Diameter, Metal Oxide Nanotubes for Trapping of Organic Molecules. *Chem. Mater.* **2015**, *27*, 1488–1494.
(32) Poncelet, O.; Skrzypski, J. Industrial Implications in the Uses of Tubular Clay Minerals. In *Developments in Clay Science*; Elsevier, **2016**; Vol. 7, pp 726–734.
(33) Paineau, E. Imogolite Nanotubes: A Flexible Nanoplatform with Multipurpose Applications. *Appl. Sci.* **2018**, *8*, 1921.
(34) Shikinaka, K. Design of Stimuli-Responsive Materials Consisting of the Rigid Cylindrical Inorganic Polymer "Imogolite." *Polym. J.* **2016**, *48*, 689–696.
(35) Liou, K.-H.; Kang, D.-Y.; Lin, L.-C. Investigating the Potential of Single-Walled Aluminosilicate Nanotubes in Water Desalination. *ChemPhysChem* **2017**, *18*, 179–183.
(36) Elliott, J. D.; Poli, E.; Scivetti, I.; Ratcliff, L. E.; Andrinopoulos, L.; Dziedzic, J.; Hine, N. D. M.; Mostofi, A. A.; Skylaris, C.-K.; Haynes, P. D.; Teobaldi, G. Chemically Selective Alternatives to Photoferroelectrics for Polarization-Enhanced Photocatalysis: The Untapped Potential of Hybrid Inorganic Nanotubes. *Adv. Sci.* **2017**, *4*, 1600153.

(37) Ma, W.; Otsuka, H.; Takahara, A. Poly(Methyl Methacrylate) Grafted Imogolite Nanotubes Prepared through Surface-Initiated ARGET ATRP. *Chem. Commun.* **2011**, *47*, 5813–5815.
(38) Yoshinaga, N.; Aomine, S. Imogolite in Some Ando Soils. *Soil Sci. Plant Nutr.* **1962**, *8*, 22–29.
(39) Karube, J. Hysteresis of the Colloidal Stability of Imogolite. *Clays Clay Miner.* **1998**, *46*, 583–585.
(40) Philipse, A. P.; Wierenga, A. M. On the Density and Structure Formation in Gels and Clusters of Colloidal Rods and Fibers. *Langmuir* **1998**, *14*, 49–54.
(41) Tsuchida, H.; Ooi, S.; Nakaishi, K.; Adachi, Y. Effects of PH and Ionic Strength on Electrokinetic Properties of Imogolite. *Colloids Surf. A - Physicochem. Eng. Asp.* **2005**, *265*, 131–134.
(42) Paineau, E.; Amara, M. S.; Monet, G.; Peyre, V.; Rouzière, S.; Launois, P. Effect of Ionic Strength on the Bundling of Metal Oxide Imogolite Nanotubes. *J. Phys. Chem. C* **2017**, *121*, 21740–21749.
(43) Kajiwara, K.; Donkai, N.; Hiragi, Y.; Inagaki, H. Lyotropic Mesophase of Imogolite,1. Effect of Polydispersity on Phase-Diagram. *Makromol. Chem.-Macromol. Chem. Phys.* **1986**, *187*, 2883–2893.
(44) Amara, M.-S.; Paineau, E.; Bacia-Verloop, M.; Krapf, M.-E. M.; Davidson, P.; Belloni, L.; Levard, C.; Rose, J.; Launois, P.; Thill, A. Single-Step Formation of Micron Long (OH)3Al2O3Ge(OH) Imogolite-like Nanotubes. *Chem. Commun.* **2013**, *49*, 11284–11286.
(45) Gustafsson, J. P. The Surface Chemistry of Imogolite. *Clays Clay Miner.* **2001**, *49*, 73–80.
(46) Teobaldi, G.; Beglitis, N. S.; Fisher, A. J.; Zerbetto, F.; Hofer, A. A. Hydroxyl Vacancies in Single-Walled Aluminosilicate and Aluminogermanate Nanotubes. *J. Phys.-Condens. Matter* **2009**, *21*, 195301.
(47) Poli, E.; Elliott, J. D.; Hine, N. D. M.; Mostofi, A. A.; Teobaldi, G. Large-Scale Density Functional Theory Simulation of Inorganic Nanotubes: A Case Study on Imogolite Nanotubes. *Mater. Res. Innov.* **2015**, *19*, S272–S282.
(48) Levard, C.; Rose, J.; Masion, A.; Doelsch, E.; Borschneck, D.; Olivi, L.; Dominici, C.; Grauby, O.; Woicik, J. C.; Bottero, J.-Y. Synthesis of Large Quantities of Single-Walled Aluminogermanate Nanotube. *J. Am. Chem. Soc.* **2008**, *130*, 5862–5863.
(49) Thill, A.; Maillet, P.; Guiose, B.; Spalla, O.; Belloni, L.; Chaurand, P.; Auffan, M.; Olivi, L.; Rose, J. Physico-Chemical Control over the Single- or Double-Wall Structure of Aluminogermanate Imogolite-like Nanotubes. *J. Am. Chem. Soc.* **2012**, *134*, 3780–3786.
(50) Mukherjee, S.; Bartlow, V. A.; Nair, S. Phenomenology of the Growth of Single-Walled Aluminosilicate and Aluminogermanate Nanotubes of Precise Dimensions. *Chem. Mater.* **2005**, *17*, 4900–4909.
(51) HuiXian, Y.; ZhaoHui, S. Individual Dispersion of Synthetic Imogolite Nanotubes via Droplet Evaporation. *Chin. Sci. Bull.* **2007**, *52*, 2301–2303.
(52) Yucelen, G. I.; Kang, D.-Y.; Schmidt-Krey, I.; Beckham, H. W.; Nair, S. A Generalized Kinetic Model for the Formation and Growth of Single-Walled Metal Oxide Nanotubes. *Chem. Eng. Sci.* **2013**, *90*, 200–212.
(53) Schindelin, J.; Arganda-Carreras, I.; Frise, E.; Kaynig, V.; Longair, M.; Pietzsch, T.; Preibisch, S.; Rueden, C.; Saalfeld, S.; Schmid, B. Fiji: An Open-Source Platform for Biological-Image Analysis. *Nat. Methods* **2012**, *9*, 676.

(54) Parsegian, V. A.; Rand, R. P.; Fuller, N. L.; Rau, D. C. Osmotic Stress for the Direct Measurement of Intermolecular Forces. In *Methods in enzymology*; Elsevier, 1986; Vol. 127, pp 400–416.
(55) Maillet, P. Structure et Croissance de Nanotubes de Ge-Imogolite Simple et Double-Paroi. PhD thesis, Université Pierre et Marie Curie-Paris VI, 2010.
(56) Dubois, M.; Zemb, T.; Belloni, L.; Delville, A.; Levitz, P.; Setton, R. Osmotic Pressure and Salt Exclusion in Electrostatically Swollen Lamellar Phases. *J. Chem. Phys.* **1992**, *96*, 2278–2286.
(57) Narayanan, T.; Sztucki, M.; Van Vaerenbergh, P.; Léonardon, J.; Gorini, J.; Claustre, L.; Sever, F.; Morse, J.; Boesecke, P. A Multipurpose Instrument for Time-Resolved Ultra-Small-Angle and Coherent X-Ray Scattering. *J. Appl. Crystallogr.* **2018**, *51*, 1511-1524.
(58) Chemmi, A.; Brendle, J.; Marichal, C.; Lebeau, B. Key Steps Influencing the Formation of Aluminosilicate Nanotubes by the Fluoride Route. *Clays Clay Miner.* **2015**, *63*, 132–143.
(59) Wada, S.; Wada, K. Effects of Substitution of Germanium for Silicon in Imogolite. *Clays Clay Miner.* **1982**, *30*, 123–128.
(60) Bishop, J. L.; Rampe, E. B.; Bish, D. L.; Abidin, Z.; Baker, L. L.; Matsue, N.; Henmi, T. Spectral and Hydration Properties of Allophane and Imogolite. *Clays Clay Miner.* **2013**, *61*, 57–74.
(61) Buining, P. A.; Philipse, A. P.; Lekkerkerker, H. N. W. Phase Behavior of Aqueous Dispersions of Colloidal Boehmite Rods. *Langmuir* **1994**, *10*, 2106–2114.
(62) Karube, J.; Nakaishi, K.; Sugimoto, H.; Fujihira, M. Electrophoretic Behavior of Imogolite under Alkaline Conditions. *Clays Clay Miner.* **1992**, *40*, 625–628.
(63) Su, C.; Harsh, J. The Electrophoretic Mobility of Imogolite and Allophane in the Presence of Inorganic Anions and Citrate. *Clays Clay Miner.* **1993**, *41*, 461–471.
(64) Arancibia-Miranda, N.; Escudey, M.; Molina, M.; Teresa Garcia-Gonzalez, M. Use of Isoelectric Point and PH to Evaluate the Synthesis of a Nanotubular Aluminosilicate. *J. Non-Cryst. Solids* **2011**, *357*, 1750–1756.
(65) Liz-Marzán, L.; Philipse, A. P. Synthesis of Platinum Nanoparticles in Aqueous Host Dispersions of Inorganic (Imogolite) Rods. *Colloids Surf. Physicochem. Eng. Asp.* **1994**, *90*, 95–109.
(66) Michot, L. J.; Bihannic, I.; Maddi, S.; Baravian, C.; Levitz, P.; Davidson, P. Sol/Gel and Isotropic/Nematic Transitions in Aqueous Suspensions of Natural Nontronite Clay. Influence of Particle Anisotropy. 1. Features of the I/N Transition. *Langmuir* **2008**, *24*, 3127–3139.
(67) Zhang, J.; Luan, L.; Zhu, W.; Liu, S.; Sun, D. Phase Behavior of Aqueous Suspensions of Mg2Al Layered Double Hydroxide: The Competition among Nematic Ordering, Sedimentation, and Gelation. *Langmuir* **2007**, *23*, 5331–5337.
(68) Michot, L. J.; Ghanbaja, J.; Tirtaatmadja, V.; Scales, P. J. Sol− Gel Transitions in Aqueous Suspensions of Synthetic Takovites. The Role of Hydration Properties and Anisotropy. *Langmuir* **2001**, *17*, 2100–2105.
(69) Cambedouzou, J.; Chorro, M.; Almairac, R.; Noé, L.; Flahaut, E.; Rols, S.; Monthioux, M.; Launois, P. X-Ray Diffraction as a Tool for the Determination of the Structure of Double-Walled Carbon Nanotube Batches. *Phys. Rev. B* **2009**, *79*, 195423.
(70) Rols, S.; Almairac, R.; Henrard, L.; Anglaret, E.; Sauvajol, J.-L. Diffraction by Finite-Size Crystalline Bundles of Single Wall Nanotubes. *Eur. Phys. J. B-Condens. Matter Complex Syst.* **1999**, *10*, 263–270.

(71) Amara, M. S.; Rouziere, S.; Paineau, E.; Bacia-Verloop, M.; Thill, A.; Launois, P. Hexagonalization of Aluminogermanate Imogolite Nanotubes Organized into Closed-Packed Bundles. *J. Phys. Chem. C* **2014**, *118*, 9299–9306.
(72) Maier, E. E.; Krause, R.; Deggelmann, M.; Hagenbuechle, M.; Weber, R.; Fraden, S. Liquidlike Order of Charged Rodlike Particle Solutions. *Macromolecules* **1992**, *25*, 1125–1133.
(73) Belamie, E.; Davidson, P.; Giraud-Guille, M. M. Structure and Chirality of the Nematic Phase in α-Chitin Suspensions. *J. Phys. Chem. B* **2004**, *108*, 14991–15000.
(74) Levitz, P.; Zinsmeister, M.; Davidson, P.; Constantin, D.; Poncelet, O. Intermittent Brownian Dynamics over a Rigid Strand: Heavily Tailed Relocation Statistics in a Simple Geometry. *Phys. Rev. E* **2008**, *78*, 030102.
(75) Israelachvili, J. N. *Intermolecular and Surface Forces*; Academic press, 2015.
(76) Mauroy, C.; Levard, C.; Moreau, C.; Vidal, V.; Rose, J.; Cathala, B. Elaboration of Cellulose Nanocrystal/Ge-Imogolite Nanotube Multilayered Thin Films. *Langmuir* **2018**, *34*, 3386–3394.
(77) Li, M.; Brant, J. A. Effects of Aluminogermanate Imogolite Nanotube Orientation on Mass Transport across Polyamide Nanocomposite Membranes. *J. Membr. Sci.* **2019**, *585*, 38–51.

Graphical abstract figure